Available online at www.sciencedirect.com
SCIENCE DIRECT®
International Journal of Heat and Mass Transfer 48 (2005) 3284–3293
International Journal of HEAT and MASS TRANSFER
www.elsevier.com/locate/ijhmt

Thermal contact resistance at low contact pressure: Effect of elastic deformation

Majid Bahrami *, M. Michael Yovanovich, J. Richard Culham

Microelectronics Heat Transfer Laboratory, University of Waterloo, Waterloo, Ont., Canada

Received 7 October 2004; received in revised form 25 February 2005

Abstract

Existing models over-predict the thermal contact resistance of conforming rough joints at low contact pressures. However, the applicable pressure range in some applications such as microelectronics cooling is low. A new model is developed which is more suitable for low pressures. The effect of elastic deformations beneath the plastically deformed microcontacts is determined by superimposing normal deformations due to self and neighboring contact spots in an elastic half-space. A parametric study reveals that the elastic deformation effect is an important phenomenon at low contact pressures. The model is compared with data and good agreement is observed at low contact pressures.

Keywords: Thermal contact resistance; Plastic/elastic deformation; Low contact pressure; Microhardness; Surface roughness

1. Introduction

The continued growth in performance and functionality of microelectronic and avionic systems has resulted in a significant increase in heat dissipation requirements and presents a great challenge to thermal engineers. The heat generated must pass through a complex network of thermal resistances to dissipate from the junction to the surroundings. A significant resistance in the network is the thermal constriction/spreading resistance through microcontacts at the interface between the package and its heat sink. An accurate knowledge of mechanics of the contact is essential for performing the thermal resistance analysis.

When random rough surfaces are placed in mechanical contact, *real contact* occurs at the summit of surface asperities which are called microcontacts. The real contact area, A_r, the summation of the microcontacts, forms a small portion of the nominal contact area, typically a few percent of the nominal contact area.

To study the constriction/spreading resistance of microcontacts, the joint is usually studied in a vacuum where the heat transfer between contacting bodies occurs only via conduction through microcontacts. Thermal contact resistance (TCR) of conforming rough surfaces in a vacuum is proportional to the real contact area [1]. TCR can be decreased by reducing the roughness and out-of-flatness of the surfaces before the interface is formed or by increasing the contact pressure. However, manufacturing highly finished surfaces is not practical due to cost constraints. Also, load constraints

* Corresponding author. Tel.: +1 519 888 4567x6181; fax: +1 519 746 9141.
E-mail addresses: majid@mhtlab.uwaterloo.ca (M. Bahrami), mmyov@mhtlab.uwaterloo.ca (M.M. Yovanovich), rix@ mhtlab.uwaterloo.ca (J.R. Culham).

0017-9310/$ - see front matter © 2005 Elsevier Ltd. All rights reserved.
doi:10.1016/j.ijheatmasstransfer.2005.02.033

Nomenclature

A	area, m^2
a	radius of microcontacts, m
b_L	specimen radius, m
c_1	Vickers microhardness coefficient, Pa
c_2	Vickers microhardness coefficient, [–]
E	Young's modulus, Pa
E'	effective elastic modulus, Pa
F	applied load, N
H_{mic}	microhardness, Pa
H^*	non-dimensional microhardness $\equiv H_{mic}/E'$
k	thermal conductivity, W/m K
L	distance between microcontacts, m
m	combined mean absolute surface slope, [–]
n	number of microcontacts
P	apparent contact pressure, Pa
R_j	thermal joint resistance, K/W
r	radial position, m
x	non-dimensional position $\equiv r/L$
Y	mean surface plane separation, m

Greek symbols

γ	plasticity index $\equiv H_{mic}/E'm$
ε	relative radius $\equiv \sqrt{A_r/A_a}$
η	density of microcontacts, m^{-2}
Λ	non-dimensional length $\equiv b_L^2/(\sigma/m)$
λ	non-dimensional separation $\equiv Y/\sqrt{2}\sigma$
σ	combined RMS surface roughness, m
υ	Poisson's ratio
ω	normal elastic deformation, m

Subscripts

0	pure plastic model value
1,2	solid 1, 2
a	apparent
r	real
s	solid, micro

on electronic components make it unfeasible to use high contact pressure.

Very little has been done for light pressures <0.1 MPa, which is the applicable range for microelectronics devices. Existing models such as [2,3] can accurately predict TCR for moderate to high contact pressures. Milanez et al. [4] experimentally studied low contact pressure joints in a vacuum and showed that the models [2,3] overestimate the TCR at low pressures. They called this phenomenon the *truncation effect* and attributed this trend to the Gaussian assumption of the surface asperities which implies that asperities with "infinite" heights exist. Milanez et al. [4] proposed correlations for maximum asperities heights as functions of surface roughness.

Existing plastic models [2,3] do not consider the effect of elastic deformations beneath the microcontacts. These effects would be negligible if the elastic modulus of contacting bodies were infinity and/or the distance between the neighboring microcontacts was small enough so the elastic deformation was the same for all microcontacts. In reality, none of the above is true and the elastic deflection underneath a microcontact is always larger than the deformation outside the microcontact area (mean plane). Mikic [5] was the first one to point out this problem and proposed a model. However, his model did not consider the effect of the elastic deformation of neighboring microcontacts and variation in the effective microhardness which was reported later by Hegazy [6]. Also Mikic did not compare his model against experimental data.

2. Problem statement

The contact between two Gaussian rough surfaces is modeled by the contact between a single Gaussian surface, that has the combined characteristics of the two surfaces, with a perfectly smooth surface. The combined roughness σ and surface slope m can be found from

$$\sigma = \sqrt{\sigma_1^2 + \sigma_2^2} \quad \text{and} \quad m = \sqrt{m_1^2 + m_2^2} \tag{1}$$

Figure 1 schematically shows the cross-section of the contact; note that the surface slopes of asperities, m, is exaggerated. In reality, the surface asperities can be visualized as shallow hills and valleys. In this study the microcontacts are assumed to deform plastically,

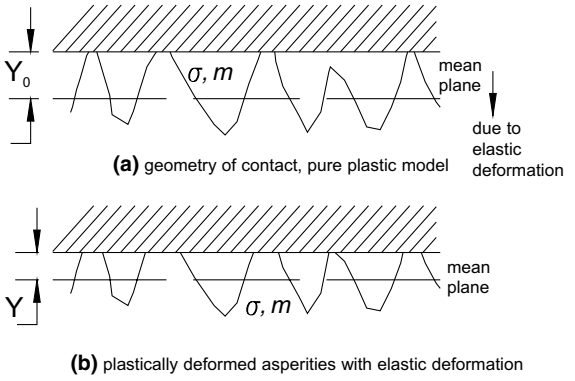

Fig. 1. Effect of elastic deformation on mean separation.

reasons supporting this assumption are discussed in the next section. Each microcontact may be visualized as a microhardness indenter. Due to the small percentage of real contact area, the contact stress within the microcontact is much larger than the compressive yield stress of the substrate. Thus, the material under the indenter consists of a zone of severe plastic deformation surrounded by a larger zone of elastic deformation. Together, these zones generate stresses that support the force exerted by the microcontact.

Consider plastically deformed microcontacts as loaded areas on an elastic half-space. The pressure applied on the microcontacts is the effective microhardness of the joint, i.e., the microhardness of the softer material in contact. As elastic deformations occur beneath the microcontacts, mean separation between the two contacting surfaces decreases, compared with the value predicted by the pure plastic model where the elastic deformation is neglected, i.e. $Y < Y_0$. As a result of smaller separation, more microcontacts are formed which in turn leads to a higher real contact area that is equivalent to a lower TCR.

The goal of this study is to investigate the effect of elastic deformations beneath the plastically deformed microcontacts on TCR. A new model is proposed that accounts for the elastic deformation of microcontacts and variation of effective microhardness with mean radius of microcontacts. A novel numerical algorithm is presented that satisfies the force balance. The present model is also compared with experimental data. The paper concludes with a critique of the present model emphasizing its merits and limitations.

3. Why plastic microcontacts?

Different approaches have been taken to analyze the deformation of asperities by assuming plastic [2], elastic [7], or elastoplastic [8,9] regimes at microcontacts. It has been observed through experiments that the real contact area is proportional to the applied load [10] which indicates an *effective microhardness* for the contact, i.e., plastic deformation of microcontacts. On the other hand, the elastic models are based on the idea that (for moving machine parts that meet millions of times during their life) the asperities may flow plastically at first, but they must reach a steady-state in which the load is supported elastically. However, if simple elastic deformation, following the Hertzian theory, is assumed for asperities, the real contact area will not be linearly proportional to the load, instead one obtains $A_r \propto F^{2/3}$. To solve this dilemma, Archard [11] proposed that the surface asperities have microasperities and microasperities have micro-microasperities and so on; by adding several levels of asperities, it can be shown that $A_r \propto F$. Greenwood and Williamson (GW) [7] developed an elastic contact model. They proposed that as the load increases new microcontacts are nucleated while the mean size of microcontacts remains constant; the GW model satisfied the observed proportionality $A_r \propto F$. As a result, an *effective elastic microhardness* can be defined for elastic models which shows that the assumption of elastic and/or plastic deformation of asperities leads to similar results [7,12]. Recently Greenwood and Wu [13] reviewed the assumptions of the GW model and concluded that "the GW definition of peaks is wrong and gives a false idea of both number and the radius of curvature of asperities". Greenwood and Wu proposed to return to the Archard idea that roughness consists of roughness on roughness and that the contact may be plastic at light loads but it becomes elastic at heavier loads. GW [7] also introduced a plasticity index as a criterion for plastic flow of microcontacts. They reported that the load has little effect on the deformation regime. GW concluded that except for especially smooth surfaces, the asperities will flow plastically under the lightest loads. Persson [14] also reported that except for polished surfaces all microcontacts deform plastically. Mikic [5] performed a thermal analysis and proposed a plasticity index $\gamma = H_{mic}/E'm$ to determine the deformation mode of asperities where the effective elastic modulus E' is defined as

$$\frac{1}{E'} = \frac{1-\upsilon_1^2}{E_1} + \frac{1-\upsilon_2^2}{E_2} \tag{2}$$

where H_{mic} is the effective microhardness. Mikic [5] concluded that for most engineering surfaces the asperity deformation mode is plastic. According to [5], the deformation mode of asperities depends on material properties E', H_{mic} and the shape of asperities m; also it is not a function of the applied load.

Rough surfaces appear to have power law spectral densities. One can think of the parameters σ and m as properties of the surface. Unfortunately, their values in practice depend on both the sampling length and the sampling interval used in the measurement. The RMS roughness σ is virtually independent of the sampling interval [15]. However, the surface slope m is sensitive to sampling interval; its value tends to increase without limit as the sampling interval is made smaller and shorter wavelengths are included. This led to the concept of functional filtering whereby both the sampling length and sampling interval are chosen to be appropriate to the particular application under consideration, see [15] for more detail. Because of this behavior, many authors used fractal descriptions to model rough surfaces [16]. The fractal model describes a surface as a large number of length scales of roughness that are superimposed on each other. According to fractal model, all contact spots of area smaller than a critical area are in plastic deformation. When load is increased, these plastically deformed spots join to form elastic spots [16]. The concept of fractal roughness has also been implemented to

electrical [17] and thermal [18] contact resistances. Majumdar and Tien [18] developed a TCR model based on fractal characteristics of roughness and compared their model with experimental data. Their model, however, over predicted the TCR data [18].

As briefly discussed above, the deformation mode of asperities has been the focus of many studies and several theories with different conclusions. A definitive conclusion for the deformation mode of the asperities has yet to be established. The general agreement within most TCR applications, as supported by experimental data, indicates a better agreement with plastic models. Bahrami et al. [1,19] collected more than 800 TCR data, conducted by many researchers during the past 40 years, and compared the data against a plastic model and observed good agreement at moderate and high loads. Therefore, in this study, the plastic deformation mode of asperities is assumed.

4. Microhardness

Microhardness can vary throughout the material as the indentation depth is increased [20]. Microhardness depends on several parameters, mean surface roughness, mean slope of asperities, method of surface preparation, and applied pressure. Depending on the surface preparation, microhardness can be much greater than the bulk hardness [6,14]. As shown in Fig. 2, microhardness decreases with increasing depth of the indenter until the bulk hardness is obtained. Hegazy [6] concluded that this increase in the plastic yield stress (microhardness) of metals near the free surface is a result of local extreme work hardening or some surface strengthening mechanism. He proposed empirical correlations to account for the decrease in microhardness with increasing depth of penetration

$$H_{\mathrm{mic}} = c_1 (d'_v/7)^{c_2} \tag{3}$$

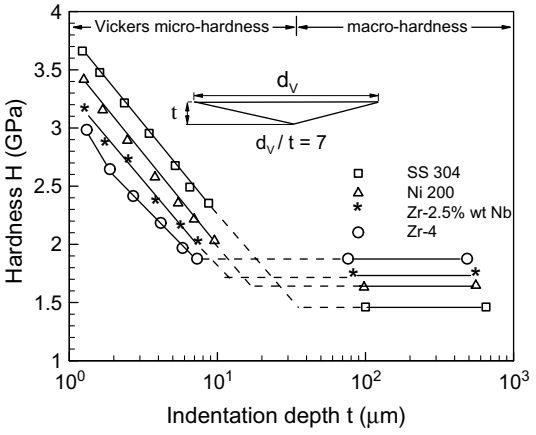

Fig. 2. Measured hardness and microhardness, Hegazy [6].

where H_{mic} is the Vickers microhardness in GPa, $d'_v = d_v/d_0$ and $d_0 = 1$ μm, $d_v = 7t$ is the Vickers indentation diagonal in μm. The correlation coefficients c_1 and c_2 are determined from Vickers microhardness measurements. Equation (3) is general and can also be used for surfaces that have a constant microhardness $H_{\mathrm{mic},e}$ by substituting $c_1 = H_{\mathrm{mic},e}$ and $c_2 = 0$. Song and Yovanovich [21] proposed a correlation to calculate H_{mic} as follows:

$$\frac{P}{H_{\mathrm{mic}}} = \left[\frac{P}{c_1 (1.62\sigma'/m)^{c_2}}\right]^{\frac{1}{(1+0.071c_2)}} \tag{4}$$

5. Present model

The present model assumes plastically deformed microcontacts and considers the effect of elastic deformation of the substrate on the contact parameters and TCR. Thus, the pure plastic model is briefly introduced in the next paragraph.

Cooper et al. (CMY) [2], based on the level-crossing theory and using the equivalent surface approximation, derived relationships for mean microcontact size a and density of microcontacts η by assuming hemispherical asperities whose heights and slopes have Gaussian distributions. Later Yovanovich [3] summarized the CMY [2] model and reported relationships for calculating the contact parameters:

$$\begin{aligned} a &= \sqrt{\frac{8}{\pi}}\left(\frac{\sigma}{m}\right)\exp(\lambda^2)\mathrm{erfc}(\lambda) \\ \eta &= \frac{1}{16}\left(\frac{m}{\sigma}\right)^2 \frac{\exp(-2\lambda^2)}{\mathrm{erfc}(\lambda)} \end{aligned} \tag{5}$$

where $\lambda = Y/\sqrt{2}\sigma$ is the dimensionless separation. They also showed that the ratio of the real contact area to the apparent area is related to the mean separation

$$\frac{A_{\mathrm{r}}}{A_{\mathrm{a}}} = \frac{P}{H_{\mathrm{mic}}} = \frac{1}{2}\mathrm{erfc}(\lambda) \tag{6}$$

where H_{mic} is the effective microhardness of the softer material in contact and $P = F/A_{\mathrm{a}}$ is the nominal contact pressure.

The modeled geometry of the contact is shown in Fig. 3. Nine microcontacts, named A to I, are shown in Fig. 3 as hatched identical circles of radius a. The microcontacts are assumed to be arranged in a square array where the shortest distance between neighboring microcontacts is L. From Fig. 3, one can find the relative radius ε as

$$\varepsilon = \sqrt{\frac{A_{\mathrm{r}}}{A_{\mathrm{a}}}} = \sqrt{\pi}\frac{a}{L} \tag{7}$$

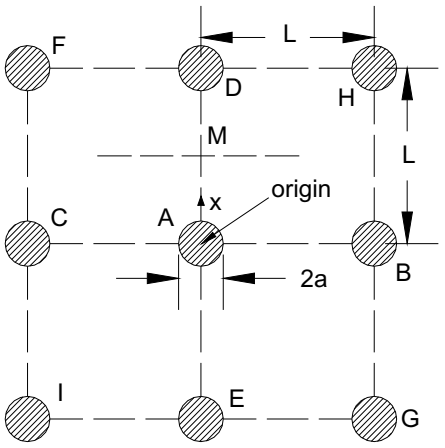

Fig. 3. Modeled geometry of contact, plan view.

The normal elastic displacement of a half-space produced as a result of applying a uniform pressure distribution H_{mic} over a circular area of radius a can be determined from [15]

$$\omega = \begin{cases} \dfrac{4H_{\text{mic}}\, a}{\pi E'} E\left(\dfrac{r}{a}\right) & r \leqslant a \\ \dfrac{4H_{\text{mic}}}{\pi E'} r\left[E\left(\dfrac{a}{r}\right) - \left(1 - \dfrac{a^2}{r^2}\right) K\left(\dfrac{a}{r}\right)\right] & r \geqslant a \end{cases} \tag{8}$$

where r is the radial location measured from the center of the loaded area; and $E(\cdot)$ and $K(\cdot)$ are the complete elliptic integrals of the second and the first kind, respectively. The mean elastic deformation of the loaded circular area is $\bar{\omega} = 16H_{\text{mic}}a/3\pi E'$.

Equation (8) can be non-dimensionalized and rearranged in the following form:

$$\omega^* = \begin{cases} \dfrac{\varepsilon}{\sqrt{\pi}} E\left(\dfrac{\sqrt{\pi}x}{\varepsilon}\right) & x \leqslant \dfrac{\varepsilon}{\sqrt{\pi}} \\ x\left[E\left(\dfrac{\varepsilon}{\sqrt{\pi}x}\right) - \left(1 - \dfrac{\varepsilon^2}{\pi x^2}\right) K\left(\dfrac{\varepsilon}{\sqrt{\pi}x}\right)\right] & x \geqslant \dfrac{\varepsilon}{\sqrt{\pi}} \end{cases} \tag{9}$$

where

$$\omega = \frac{4H_{\text{mic}}L}{\pi E'}\omega^* = \frac{4H_{\text{mic}}a}{\sqrt{\pi}E'\varepsilon}\omega^* \tag{10}$$

and $x = r/L$. The relationship for the deformation outside the contact area, i.e., $x \geqslant \varepsilon/\sqrt{\pi}$ is complex as given in Eq. (9). The following simpler relationship can be used to calculate the deformation of a half-space outside the loaded area

$$\omega^* = \frac{0.26\ \varepsilon^2}{x} \quad x \geqslant \frac{\varepsilon}{\sqrt{\pi}} \tag{11}$$

The line AM, in Fig. 3, is chosen as a representative (or mean plane) of the half-space to estimate the total elastic deformations due to microcontacts A to I. The elastic deformation of the mean plane AM can be calculated using superposition. The non-dimensional mean elastic deformation underneath the microcontact A due to its neighbors and itself is

$$\overline{\omega_1^*} = \underbrace{\frac{4\varepsilon}{3\sqrt{\pi}}}_{\text{due to A}} + \underbrace{0.52\pi \int_0^{\frac{\varepsilon}{\sqrt{\pi}}} \sum \frac{x}{a_i x + b_i}\mathrm{d}x}_{\text{due to neighbors}} \quad x \leqslant \frac{\varepsilon}{\sqrt{\pi}} \tag{12}$$

where a_i and b_i are the constants due to changing the location of the origin from each neighboring microcontact to the center of the microcontact "A". Using the same method, the mean deformation for the rest of the mean plane AM can be expressed as:

$$\overline{\omega_2^*} = \frac{0.52\varepsilon^2}{\dfrac{1}{4} - \dfrac{\varepsilon^2}{\pi}} \int_{\frac{\varepsilon}{\sqrt{\pi}}}^{1/2} \sum \frac{x}{a_i x + b_i}\mathrm{d}x \quad \frac{\varepsilon}{\sqrt{\pi}} \leqslant x \leqslant \frac{1}{2} \tag{13}$$

Finally the mean elastic deformation of the mean plane AM is determined by taking a weighted average of $\overline{\omega_1^*}$ and $\overline{\omega_2^*}$. Figure 4 shows the mean deformation due to microcontact A only, total mean deformation considering the effects of neighbors, and the net elastic displacement for the microcontact "A" as the relative radius of microcontacts ε varies. As expected, for small values of $\varepsilon < 0.01$ (relatively low contact pressure) the effects of neighboring microcontacts is small and can be ignored. As ε increases, the effect of neighboring microcontacts becomes more significant, also the displacement of the mean plane increases. As a result of these two competing trends, the net elastic deformation beneath the microcontact "A" becomes smaller and eventually the net displacement approaches zero at relatively large loads.

A new numerical model is developed to account for the elastic deformation beneath microcontacts and vari-

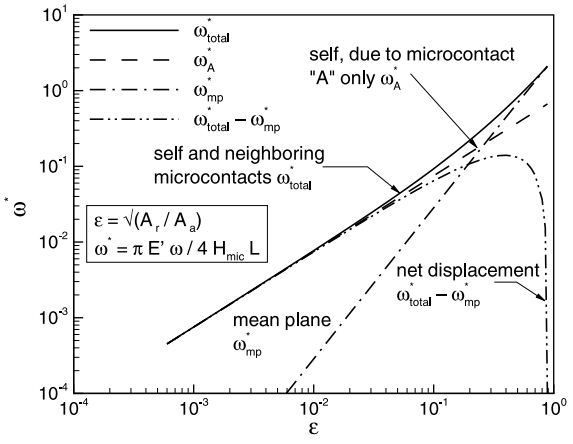

Fig. 4. Elastic deformation beneath microcontact A, for $0 < x < \varepsilon/\sqrt{\pi}$.

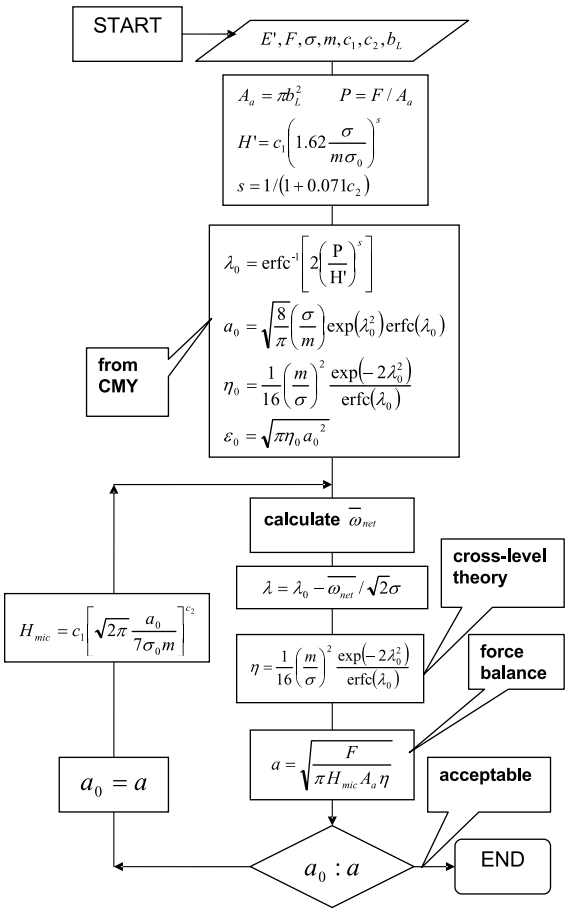

Fig. 5. Numerical algorithm used in present model.

ations in microhardness. The numerical algorithm used in the present model is described below and is shown in Fig. 5.

Cooper et al.'s (CMY) [2] relationships, Eqs. (5) and (6) are used to calculate the mean radius a_0, density η_0, relative radius ε_0, and mean separation of the joint λ_0. Song and Yovanovich's correlation [21], Eq. (4), is employed to estimate an effective microhardness H' for the pure plastic model. The subscript 0 indicates the pure plastic model values.

The net mean elastic deformation, $\omega_{\mathrm{net}} = \omega_1 - \omega_{\mathrm{AM}}$, is then calculated using relative radius ε_0 as described in the previous section. A new mean separation between contacting surfaces can be found from, $\lambda = \lambda_0 - \omega_{\mathrm{net}}/\sqrt{2}\sigma$. With new separation λ, one can determine a new density of microcontacts η from Eq. (5). Applying a force balance, a new mean radius of microcontacts a is determined from, $a = \sqrt{F/\pi H_{\mathrm{mic}} A_{\mathrm{a}} \eta}$. Since the mean radius of the microcontacts changes as the applied load varies, microhardness will also change according to Eq. (3). If the print area in a Vickers test is assumed to be equal to the microcontact area, a relation between the Vicker's diagonal and the mean size of microcontacts can be found as, $d_v = \sqrt{2\pi}a$. Therefore, a new effective microhardness can be computed using the new radius of microcontacts. This procedure continues until the difference between the new mean radius of microcontacts a and the old one a_0 becomes negligible.

The results of the above procedure are used to calculate the TCR of the joint. The thermal resistance analysis is based on the premise that there are n ($=\eta A_{\mathrm{a}}$) identical circular microcontacts of radius a that provide n parallel paths for thermal energy to be transferred in the contact plane. The constriction/spreading resistance of the joint can be determined by employing the flux tube solution [2] as:

$$R_{\mathrm{j}} = \frac{(1-\varepsilon)^{1.5}}{2k_{\mathrm{s}} a \eta A_{\mathrm{a}}} \tag{14}$$

where $k_{\mathrm{s}} = 2k_1k_2/(k_1 + k_2)$ is the harmonic mean of thermal conductivities of the contacting bodies.

6. Parametric study

The present model is run for a typical joint as the applied load is varied over a wide range to study the trends of the contact parameters; see Figs. 6 and 7 for the contact input parameters of the studied joint. The contact parameters calculated by both the present and the pure plastic models are listed in Table 1.

Figures 6 and 7 show the ratio of the contact parameters as the non-dimensional pressure P/H_{mic} is increased. As shown in these plots, the ratio of separations λ_0/λ is greater than one for the entire comparison due to elastic deformations of the substrate. As a result of smaller separation, more microcontacts are formed $n/n_0 > 1$, the real contact area $A_{\mathrm{r}}/A_{\mathrm{r0}}$ is increased, thus

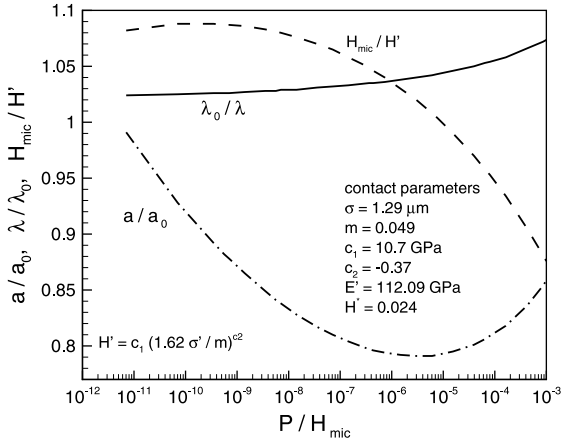

Fig. 6. Ratio of calculated values by present model over pure plastic model for: mean separation, mean radius of microcontacts, and effective microhardness.

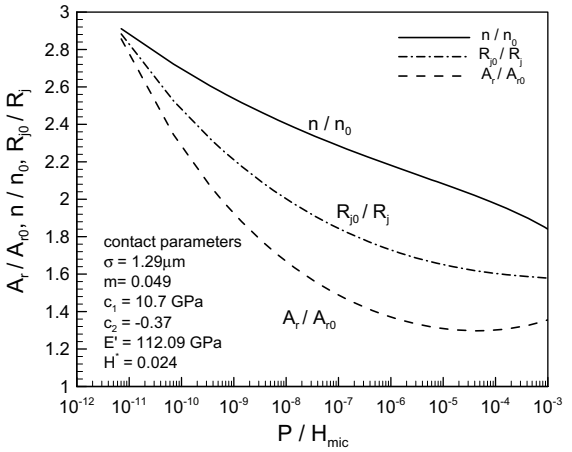

Fig. 7. Ratio of calculated values by present model over pure plastic model for: density of microcontacts, real contact area, and TCR.

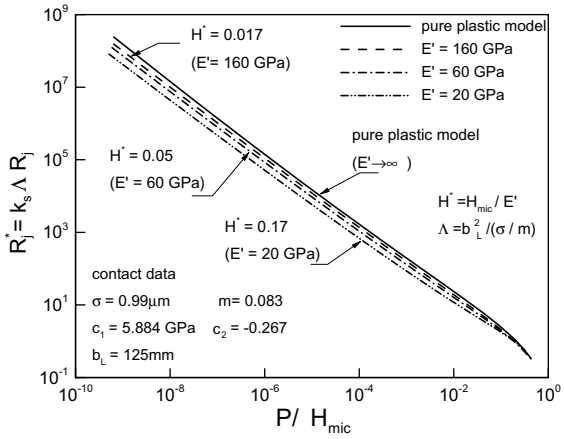

Fig. 8. Effect of elastic modulus E' on present model.

thermal resistance is decreased $R_{j0}/R_j > 1$. It can be seen that these ratios A_r/A_{r0}, n/n_0, and R_{j0}/R_j decrease as the applied load increases which indicates that the elastic deformation effect becomes less important at higher loads. This is consistent with the trend seen in Fig. 4.

Figure 6 shows that the ratio of microcontacts radius $a/a_0 < 1$ throughout the comparison. However, it should be noted that the absolute radius of microcontacts, a, increases by increasing the load, see Table 1. Therefore, the effective microhardness H_{mic} decreases as the load increases, see Fig. 2. The effective microhardness shown in Fig. 6 is non-dimensionalized with respect to $H' = c_1(1.62\sigma/m)^{c_2}$ which remains constant throughout the comparison.

Non-dimensional joint resistances of a typical joint is shown in Fig. 8 over a wide range of the non-dimensional pressure P/H_{mic}. Four values of $E' = 20$, 60, 160 GPa, and ∞ (pure plastic model) have been selected to investigate the effect of elastic modulus, E', on TCR. Other contact input parameters are shown in the figure and are kept constant as the effective elastic modulus E' is changed. The ratio of the effective microhardness over the effective elastic modulus $H^* = H_{mic}/E'$ is used to label these four curves. It can be seen that as H^* approaches zero, i.e. $E' \to \infty$, the present model approaches the pure plastic model and the elastic effect vanishes. Therefore, it may be concluded that the non-dimensional parameter H^* is a measure of how important is the elastic deformation effect. Also note that the difference between the present model and the pure elastic model decreases as P/H_{mic} (contact pressure) increases.

Table 1
Contact parameters calculated by present and pure plastic models

$F(N)$	Pure plastic model				Present model			
	λ_0	ε_0	a_0 (μm)	η_0	λ	ε	a (μm)	η
0.001	4.88	1.57E−06	4.76	0.03	4.77	2.66E−06	4.71	0.10
0.01	4.63	5.47E−06	5.01	0.38	4.52	8.38E−06	4.65	1.03
0.1	4.36	1.89E−05	5.31	4.03	4.25	2.65E−05	4.66	10.31
1	4.07	6.45E−05	5.66	41.34	3.96	8.41E−05	4.74	100.13
5	3.87	1.51E−04	5.94	205.94	3.75	1.89E−04	4.86	481.16
10	3.77	2.18E−04	6.08	408.69	3.66	2.68E−04	4.93	940.72
50	3.55	5.07E−04	6.44	1975.29	3.43	6.03E−04	5.13	4396.62
100	3.45	7.28E−04	6.61	3864.60	3.33	8.57E−04	5.25	8481.07
200	3.35	1.05E−03	6.80	7524.41	3.23	1.22E−03	5.38	16282.06
1000	3.10	2.41E−03	7.30	34627.84	2.97	2.76E−03	5.78	72497.73
2000	2.99	3.44E−03	7.55	66171.48	2.86	3.93E−03	6.00	136509.5
5000	2.84	5.51E−03	7.91	154167.2	2.70	6.27E−03	6.34	311572.4
10,000	2.71	7.85E−03	8.23	289821.9	2.58	8.95E−03	6.65	575983.1
20,000	2.59	1.12E−02	8.58	540371.2	2.45	1.28E−02	7.03	1054370
50,000	2.42	1.78E−02	9.13	1213824	2.27	2.05E−02	7.63	2303327

Beyond a certain pressure the difference between the pure plastic model and the present model (three values of E') becomes negligible. This is in agreement with the observed trend in Fig. 4 which indicates that the effect of elastic deformation is more important at lighter loads.

7. Comparison with data

The present model is compared with experimental data of Milanez et al. [4] in Figs. 9–11. They collected three sets of data for SS 304, the surface parameters of each test are listed in the corresponding plot. These data sets differ only in roughness levels which are 0.72, 1.29, and 3.07 μm. The pure plastic model is also included in the comparisons to better show the effect of elastic deformation. The averaged difference between the present model and the pure plastic model over the applied load range is also reported in the plots. Moreover, the non-dimensional parameter H^* is shown for each set of data where H_{mic} is an average value of the effective microhardness over the comparison range. As shown in the plots, the data of [4] show a better agreement with the present model at relatively low loads and move toward the pure plastic model at higher loads.

The present model is also compared with experimental data of Hegazy [6] in Figs. 12–14. Hegazy conducted several experiments with four different alloys. Here, three different materials are chosen: Zr—2.5%wt., Zircaloy 4, and Nickel 200. The data cover a relatively wide range of contact input parameters: elastic modulus E', roughness σ, thermal conductivity k_s, and

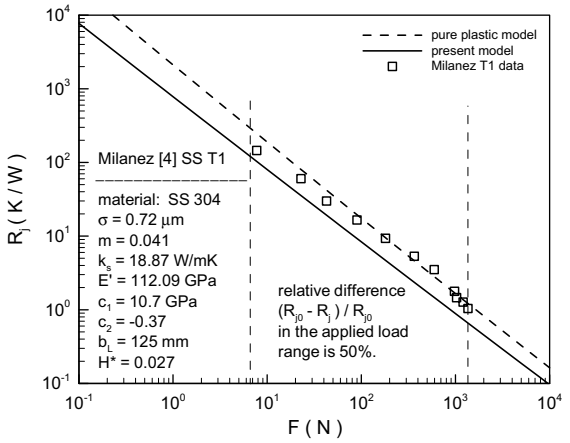

Fig. 9. Comparison of present model with Milanez et al. [4] data, test T1.

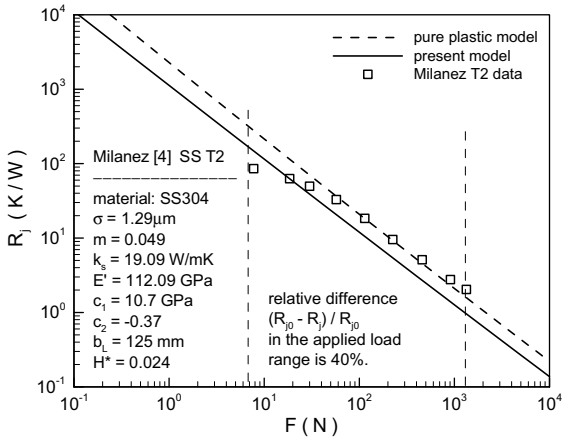

Fig. 10. Comparison of present model with Milanez et al. [4] data, test T2.

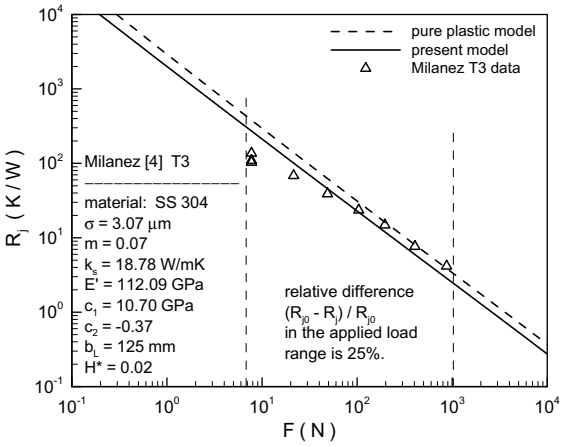

Fig. 11. Comparison of present model with Milanez et al. [4] data, test T3.

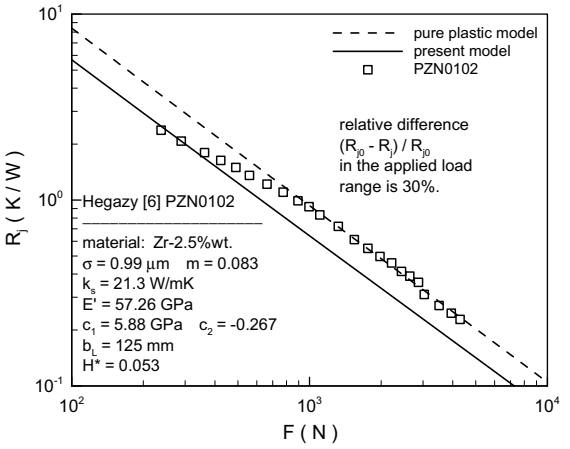

Fig. 12. Comparison of present model with Hegazy [6] data, test PZN0102.

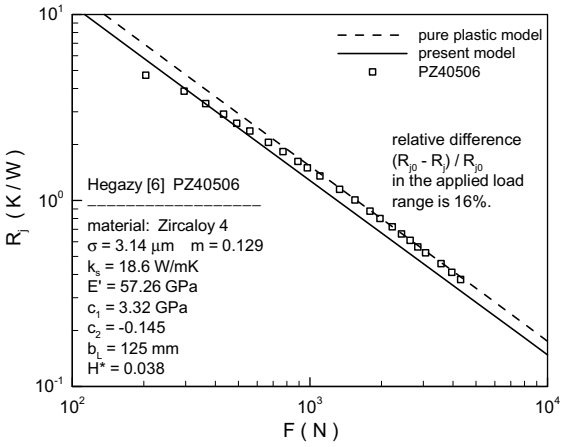

Fig. 13. Comparison of present model with Hegazy [6] data, test PZ40506.

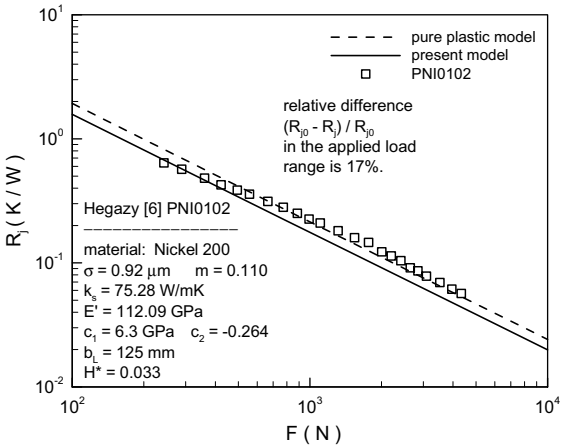

Fig. 14. Comparison of present model with Hegazy [6] data, test PNI0102.

microhardness coefficients c_1 and c_2. The material properties and surface parameters are listed in the figures. Similar to [4] data, the data of [6] are closer to the present model at smaller loads and move toward the pure plastic model at larger loads.

8. Conclusion

The effect of elastic deformation of the substrate underneath the microcontacts is studied on the TCR of rough conforming joints in a vacuum, where the microcontacts are assumed to deform plastically. The present model accounts for elastic deformations of the substrates due to self and neighboring microcontacts using superposition of elastic deformations in a half-space. The present model also accounts for the variation in the effective microhardness and satisfies the force balance.

The microcontacts are assumed as identical circles which are arranged in a square array. Relationships are derived for the average normal elastic deformation of the elastic substrate beneath microcontacts. The net elastic deformation of the microcontacts is calculated. Using the level-crossing theory, the mean separation between two contacting bodies is modified for the net elastic deformation. An iterative numerical algorithm is developed to compute the modified mean size, density, and the contact resistance of the joint.

The trends of the present model are studied and compared with the pure plastic model where the elastic deformation is completely ignored. It is observed that as a result of the elastic deformation the mean separations between two contacting surfaces becomes smaller; thus

- more microcontacts are nucleated,
- the real contact area is increased, and
- thermal contact resistance is decreased.

It is also shown that the elastic deformation effect becomes less important at higher loads. This is a result of the fact that the net elastic deformation approaches zero at relatively high loads, i.e., the elastic deformation becomes uniform for the entire mean plane.

A non-dimensional parameter $H^* = H_{\mathrm{mic}}/E'$ is introduced as a measure of importance of the elastic deformation. As H^* approaches zero ($E' \to \infty$) the present model approaches the pure plastic model. It is also shown that for a fixed contact, the elastic effect is more significant at smaller roughness levels.

The present model is compared against experimental data of [4,6]. The experimental data cover a relatively wide range of input contact parameters. The data show a better agreement with the present model at low contact loads. The data, however, move toward the pure plastic model at high contact loads.

It should be noted that the present model assumes a mean uniform size and a square distribution for microcontacts. As a result, the effect of elastic deformation of the substrate is to decrease the mean separation Y between the contacting bodies which leads to an increase in the number of microcontacts. The model, however, does not predict any effect of clustering due to larger wavelength components in the roughness which may occur in some contacts. In addition, the present model tends to under predict TCR for moderate to high contact pressures.

Acknowledgement

The authors gratefully acknowledge the financial support of the Centre for Microelectronics Assembly

and Packaging, CMAP and the Natural Sciences and Engineering Research Council of Canada (NSERC).

References

[1] M. Bahrami, J.R. Culham, M.M. Yovanovich, Thermal contact resistance: a scale analysis approach, ASME Journal of Heat Transfer 126 (6) (2004) 896–905.
[2] M.G. Cooper, B.B. Mikic, M.M. Yovanovich, Thermal contact conductance, Int. J. Heat Mass Transfer 12 (1969) 279–300.
[3] M.M. Yovanovich, Thermal contact correlations, in: T.E. Horton (Ed.), Progress in Aeronautics and Aerodynamics: Spacecraft Radiative Transfer and Temperature Control, vol. 83, 1982, pp. 83–95 (Also AIAA Paper no. 81-1164).
[4] F.H. Milanez, M.M. Yovanovich, M.B.H. Mantelli, Thermal contact conductance at low contact pressures, AIAA J. Thermophys. Heat Transfer 18 (2003) 37–44.
[5] B.B. Mikic, Thermal contact conductance; theoretical considerations, Int. J. Heat Mass Transfer 17 (1974) 205–214.
[6] A.A. Hegazy, Thermal joint conductance of conforming rough surfaces: Effect of surface micro-hardness variation, Ph.D. thesis, University of Waterloo, ON, Canada, 1985.
[7] J.A. Greenwood, B.P. Williamson, Contact of nominally flat surfaces, Proc. R. Soc. London A295 (1966) 300–319.
[8] W.R. Chang, I. Etison, D.B. Bogy, An elastic–plastic model for the contact of rough surfaces, ASME J. Tribol. 109 (1987) 253–257.
[9] Y. Zhao, D.M. Maietta, L. Chang, An asperity model incorporating the transition from elastic deformation to fully plastic flow, ASME J. Tribol. 122 (2000) 86–93.
[10] D. Tabor, The Hardness of Metals, Oxford University Press, Amen House, London, 1951.
[11] J.F. Archard, Contact and rubbing of flat surface, J. Appl. Phys. 24 (1953) 981–988.
[12] J.A. Greenwood, J.H. Tripp, The elastic contact of rough spheres, ASME J. Appl. Mech. 89 (1) (1967) 153–159.
[13] J.A. Greenwood, J.J. Wu, Surface roughness and contact: An apology, Meccanica 36 (2001) 617–630.
[14] B.N.J. Persson, Sliding Friction Physical Principles and Applications, Springer, Berlin, Germany, 2000.
[15] K.L. Johnson, Contact Mechanics, Cambridge University Press, Cambridge, 1985.
[16] A. Majumdar, B. Bhushan, Role of fractal geometry in roughness characterization and contact mechanics of surfaces, ASME J. Tribol. 112 (1990) 205–216.
[17] Y.H. Jang, J.R. Barber, Effect of contact statistics on electrical contact resistance, J. Appl. Phys. 94 (2003) 7215–7221.
[18] A. Majumdar, C.L. Tien, Fractal network model for contact conductance, ASME J. Heat Transfer 113 (1991) 516–525.
[19] M. Bahrami, J.R. Culham, M.M. Yovanovich, G.E. Schneider, Review of thermal joint resistance models for non-conforming rough surfaces, ASME J. Appl. Mech. Rev. (to appear) (Also ASME Conference Paper no. HT2003-47051).
[20] M.M. Yovanovich, E.E. Marotta, Thermal spreading and contact resistances, in: A. Bejan, D. Kraus (Eds.), Heat Transfer Handbook, John Wiley and Sons Inc., Hoboken, New York, 2003, Chapter 4.
[21] S. Song, M.M. Yovanovich, Relative contact pressure: dependence on surface roughness and Vickers microhardness, AIAA J. Thermophys. Heat Transfer 2 (1) (1988) 43–47.